3-D RESISTIVITY INVERSION MODELS OF MT ARRAY DATA IN THE TAUPO VOLCANIC ZONE, NEW ZEALAND

Edward A. Bertrand[1], Nathaniel J. Lindsey[2], T. Grant Caldwell[1], Gregory A. Newman[2] and Erika Gasperikova[2]

[1]GNS Science, 1 Fairway Drive, Avalon, Lower Hutt 5010, New Zealand

[2]Lawrence Berkeley National Laboratory, Earth Sciences Division, Berkeley, California, USA

t.bertrand@gns.cri.nz

Keywords: *Magnetotellurics, Geothermal, Taupo Volcanic Zone, 3-D Inversion.*

ABSTRACT

Independent 3-D resistivity inversion models of magnetotelluric (MT) array data located in the Taupo Volcanic Zone (TVZ), New Zealand, have been generated using WSINV3DMT (Siripunvaraporn et al., 2005) and a preconditioned non-linear conjugate gradient algorithm EMGeo (Newman and Alumbaugh, 2000) implemented on a multi-thousand core machine at Lawrence Berkeley National Laboratory. Previously, 2-D and 3-D inversion models of subsets of the total MT array data have imaged the resistivity structure of the upper crust beneath the TVZ, and have resolved quasi-vertical low-resistivity plumes that connect shallow geothermal fields to an inferred magmatic heat source that lies below the brittle-ductile transition at ~6-8 km depth (Bertrand et al., 2012; 2013). The TVZ in the central North Island of New Zealand is the largest rhyolitic magmatic system on Earth and hosts more than 20 high-temperature liquid-dominated geothermal systems (Bibby et al., 1995; Wilson et al., 1995).

Here, we focus on assessing two independent 3-D resistivity inversion models generated using the WSINV3DMT and EMGeo algorithms, each implemented with different control parameters (e.g. error-floors, data-weights, model mesh etc.). We use 3-D inversion models from each code to compute synthetic MT phase tensors for comparison with the measured values. By comparing the synthetic and measured phase tensors, we can efficiently visualize the model fit at all sites in the array, at each period. In this way we can assess the robustness of resistivity structures contained in these MT inversion models and gain insight as to how the different inversion implementations affect the model results.

1. INTRODUCTION

MT is a passive geophysical imaging technique that records the time variation of natural electric and magnetic fields at the surface of the Earth. The amplitude and phase of these field components at the surface are dependent on the subsurface electrical structure. Specifically, ratios of simultaneous electric and magnetic field measurements are used to image spatial variations of the electrical resistivity in the Earth. The electrical resistivity ρ (or its reciprocal quantity, the electrical conductivity σ) is highly sensitive to the fluid content of crustal and upper mantle rocks (e.g. Unsworth, 2010). In the geothermal industry, MT is routinely used to generate models of the subsurface resistivity structure. These resistivity inversion models (combined with other data) can be interpreted to understand the deep fluid pathways that supply heat to the geothermal fields (e.g. Bertrand et al., 2013).

In the central North Island of New Zealand, the Taupo Volcanic Zone (TVZ) is an actively-rifting volcanic arc (Wilson et al., 1995) that hosts more than 20 high-temperature liquid-dominated geothermal systems. Bibby et al. (1995) described the shallow (< 3 km) geothermal fields as the upper portion of rising, high-temperature convection plumes that extend down to an underlying magmatic heat source below the brittle-ductile transition. In 2008, the government of NZ funded an integrated research program (Hotter and Deeper Exploration Science; Bignall 2010) to explore the upper crustal structure on a regional-scale beneath the TVZ. This project included passive-seismic (Bannister et al., 2013) and MT data acquisition (Figure 1) to investigate links between the deep magmatic heat sources and the shallow hydrothermal systems. The initial MT measurements were located in the southeastern part of the TVZ (black box in Figure 1).

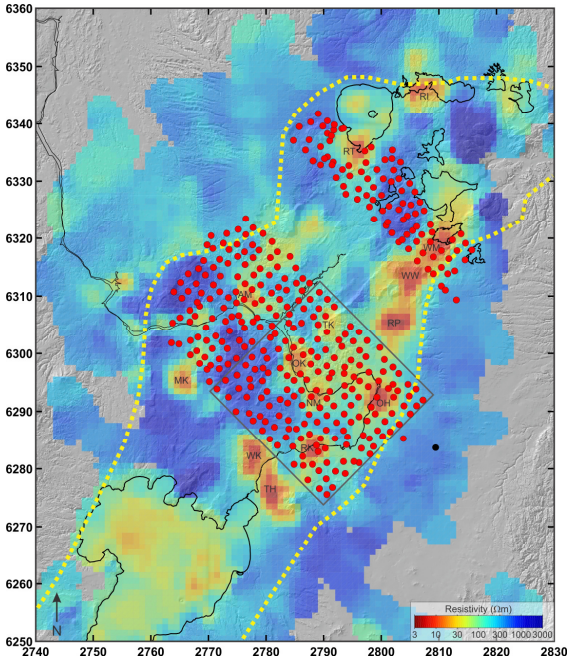

Figure 1: Map of MT data in the southeastern TVZ. Red circles show broadband MT sites with data included in the 3-D modeling below bounded by the grey square. The background digital elevation model is overlain by the DC apparent resistivity map (Bibby et al., 1995) that correlates low resistivity zones to geothermal systems: TH Tauhara, WK Wairakei, RK Rotokawa, MK Mokai, NM Ngatamariki, OK Orakei-Korako, OH Ohaaki, TK Te Kopia, AM Atiamuri, RP Reporoa, WW Waiotapu-Waikiti, WM Waimangu, RT Rotorua and RI Rotoiti. Yellow lines show the approximate boundaries of the young TVZ after Wilson et al., 1995.

The goal of these MT measurements was to provide a comprehensive picture of electrical resistivity structures down to the brittle-ductile transition, in order to advance our understanding of the processes that transport heat to the surface. Initial 2-D and 3-D resistivity inversion models from these MT data provided the first-ever geophysical images of convection plumes that link several of the shallow geothermal fields to deeper low-resistivity zones (Bertrand et al., 2012; 2013). Since completion of the initial MT data acquisition campaign (220 measurements), GNS Science has collected additional MT data to expand the array coverage towards the western margin of the TVZ, and to include the Rotorua and Waimangu geothermal systems (Heise et al., 2014). The total MT database now includes 397 measurements (Figure 1).

2. MT DATA ANALYSIS

2.1 Distortion and the MT Phase Tensor

Localized conductivity heterogeneities beneath an MT site can alter the direction and magnitude of the regional electric fields. At long-periods (i.e. skin-depth greater than the dimensions of local heterogeneities), inductive effects within these conductive heterogeneities become negligible compared to the inductive response of regional structure (e.g. Jiracek, 1990). Therefore, MT data comprise a superposition of the inductive (frequency dependent) signature of the regional structure and the galvanic (frequency independent) distortion from any localized near-surface heterogeneities (Wannamaker et al., 1984). This distortion will mask the magnitude of the regional response and further analysis is required to eliminate the galvanic effects. In tensor notation,

$$\mathbf{D} = \begin{bmatrix} D_{11} & D_{12} \\ D_{21} & D_{22} \end{bmatrix} \tag{2.0}$$

defines the distortion tensor whose elements are real and frequency independent (e.g. Groom and Bahr, 1992; Chave and Smith, 1994). The relationship between the regional ($\mathbf{Z}_R$) and observed ($\mathbf{Z}$) impedance tensors is,

$$\mathbf{Z} = \mathbf{D}\mathbf{Z}_R . \tag{2.1}$$

To eliminate the galvanic distortion requires the determination of $\mathbf{Z}_R$ from the measured tensor $\mathbf{Z}$. However, equation (2.1) defines an underdetermined set of eight equations with twelve unknowns, requiring the introduction of constraints to obtain a solution.

Several techniques have been developed to extract the regional impedance tensor based on the underlying assumption that the subsurface resistivity structure is two-dimensional. In the unknown geoelectric strike coordinate frame, only the off-diagonal components of the impedance tensor are non-zero. Early models (e.g. Swift, 1967; reprinted 1986; Zhang et al., 1987; Bahr, 1988) estimate the geoelectric strike from a minimization criterion through rotation of the observed impedance tensor. However, rotational methods are unstable for measured data containing noise and/or strong distortion and can lead to poor estimates of strike. Groom and Bailey (1989) proposed a tensor decomposition model that uses an inversion scheme to remove the non-inductive responses from the impedance tensor. The algorithm was extended by McNeice and Jones (2001) to statistically fit an entire dataset simultaneously, and is based on factoring the distortion tensor into determinable (twist and shear angles that depend on the coordinate system and are functions of the constraints imposed) and non-determinable (anisotropy and site-gain) components. This formulation manifests as a set of 8 equations and 7 unknowns (the geoelectric strike, the twist and shear angles, and the 4 components of the 2-D impedance tensor) that is solved using a least-squares approach. While equation (2.1) necessarily requires constraints to obtain a full solution, the assumptions made by Groom and Bailey (1989) reduce the problem to a degree where it becomes over-determined. This in itself suggests that too many constraints have been applied.

Caldwell et al. (2004) showed that it is possible to separate out the distortion independent part of the impedance tensor without imposing any assumptions regarding the dimensionality of the regional conductivity structure. Expressing the impedance tensor in real (X) and imaginary (Y) parts,

$$\mathbf{Z} = \mathbf{X} + i\mathbf{Y} \tag{2.2}$$

the MT phase tensor is defined to be,

$$\mathbf{\Phi} = \mathbf{X}^{-1}\mathbf{Y} = \begin{bmatrix} \Phi_{11} & \Phi_{12} \\ \Phi_{21} & \Phi_{22} \end{bmatrix}. \tag{2.3}$$

It follows from equation (2.1) that $\Phi = \Phi_R$. Therefore, the observed and regional phase tensors are identical and independent of galvanic distortion (Caldwell et al., 2004; Bibby et al., 2005). The four elements of the phase tensor are the only uniquely determinable portion of the regional impedance tensor and themselves yield information on the data dimensionality and regional conductivity structure. This information can be visualized by representing the phase tensor as an ellipse that is completely characterized by one direction α, and three coordinate invariants, Φ_{max}, Φ_{min}, and β. The phase tensor is therefore a property of the measured MT impedance tensor and is resistant to distortion from unresolvable local structure (Booker, 2013).

2.2 MT Data Dimensionality

Prior to inversion modeling, careful dimensionality analysis must be completed to determine if a 1-D, 2-D or 3-D interpretation is needed. Simplified analysis of MT data in dimensions lower than required can lead to artifacts in inversion models and erroneous interpretations (Simpson and Bahr, 2005). Most often a 1-D approach is insufficient and MT data are routinely modeled using a 2-D or 3-D approximation. The phase tensor skew angle β measures deviation from 2-Dimensionality and is plotted for a 169 site subset of the total MT array data in Figure 2. Non-zero β values and variations in the orientation of the phase tensor ellipses indicate the presence of 3-D structure (Caldwell et al., 2004). Figure 2 shows that at short periods, β is near-zero indicating that these data are 1-D or 2-D. However, at longer periods β is $> 3°$ and these data clearly reflect 3-D resistivity structure.

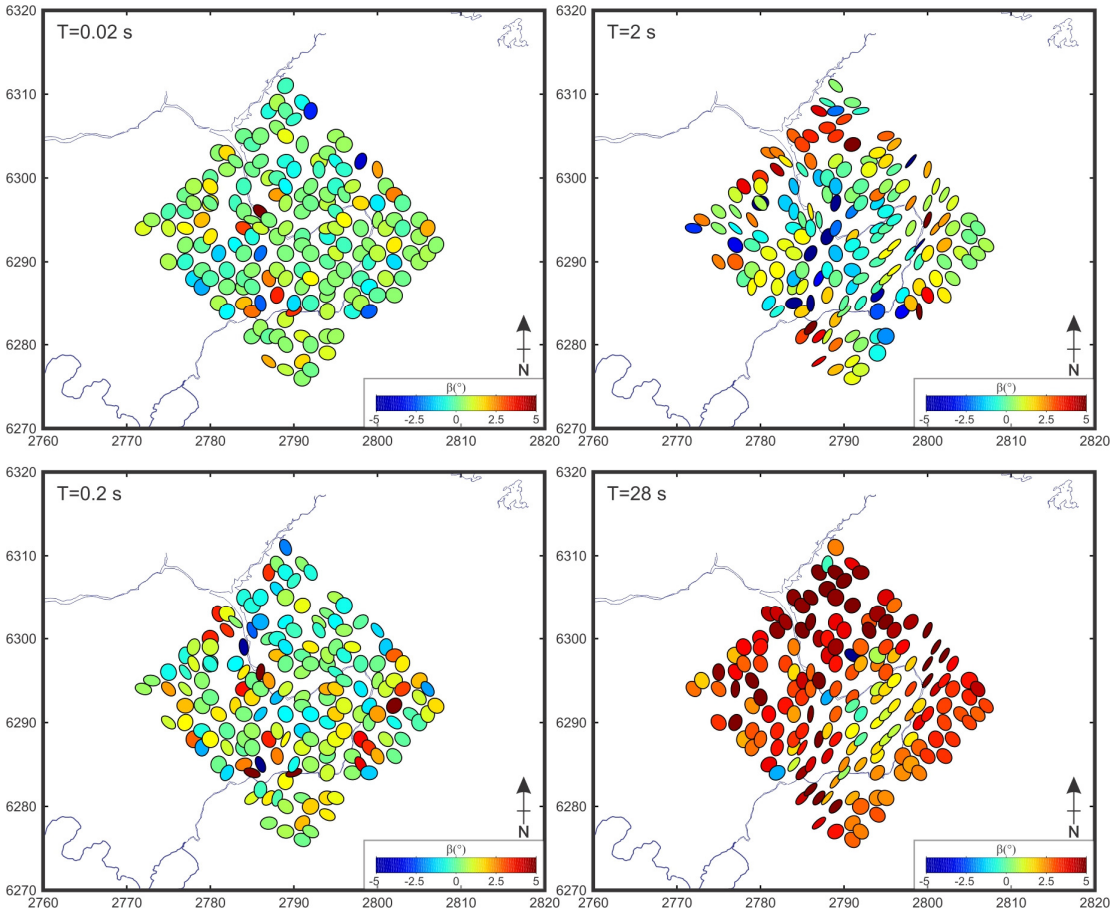

Figure 2: Plots showing the phase tensor skew angle β. Values of β > 3° indicate the presence of 3-D electrical structure.

2.3 3-D Inversion Modeling

For MT data that display 3-D effects but maintain an overall 2-D characteristic, inversion using a 2-D algorithm can be valid (Wannamaker, 1999; Ledo, 2005). However, since the public release in 2005 of the 3-D inversion algorithm WSINV3DMT (Sirapunvarapon et al., 2005), and the more recent public release of ModEM (Egbert and Kelbert, 2012; Kelbert et al., 2014), 3-D interpretation of MT data has rapidly developed in the MT research community (e.g. Tuncer et al., 2006; Heise et al., 2008). Despite progress towards 3-D modeling, the extensive computational demands have limited the routine application of 3-D inversion modeling with non-parallelized algorithms and standard desktop computers.

In this paper we compare two independent 3-D inversion models of subsets of the total MT array data in the TVZ (black box in Figure 1). One inversion model was generated using the serial version of WSINV3DMT, referred to hereafter as the WS-model. The second inversion model (EMGeo-model) was generated using a preconditioned, non-linear conjugant gradient algorithm (EMGeo; Newman and Alumbaugh, 2000) that is massively-parallelized and implemented on several thousand cores of the NERSC (National Energy Research Scientific Computing Centre) Cray XT4 Hopper system at Lawrence Berkeley National Laboratory (LBNL).

Comparing models from independent inversion algorithms is not a simple task. Since all geophysical inversion models are ill-conditioned, owing to a greater number of model parameters than data points, an infinite number of models exist that can equally well fit the measured data. This seemingly disastrous fact is overcome by imposing constraints to regularize the inversion problems. In MT, Tikhonov regularization (Tikhonov and Arsenin, 1977) is used to condition the inversion towards smooth or minimum structure models. Since MT measurements can be thought of as sampling hemispherical volumes with a radius given by the skin-depth δ, where

$$\delta \approx 503\sqrt{\rho T} \qquad (2.4)$$

is the skin depth in metres, ρ is the electrical resistivity and T is the period, resistivity structures influence adjacent measurements when the inductive length-scale (i.e. the skin-depth) becomes larger than the site spacing. Thus, smooth models are appropriate.

Here we assess the overall fit of these inversion models by computing synthetic MT data for each model result, calculating phase tensors from these synthetic data, and generating misfit tensor ellipses (Heise et al., 2007; 2013) between the synthetic and measured data. Comparing predicted and observed phase tensors is an excellent way to assess modeling success (Booker, 2013) as these data are not influenced by distortion from local structure.

3. 3-D MODEL COMPARISON

3.1 WS-Model

The 3-D inversion algorithm WSINV3DMT was used to generate a 3-D resistivity inversion model of a 169-site subset of the MT array data in the TVZ. A total of 18 periods were inverted, using 4 periods per decade between

0.01 s and 1000 s. The model mesh was rotated 45° to align cell boundaries with the geoelectric-strike (N45°E) of the TVZ, and in this strike-coordinate system, fixed error floors of 20% for the diagonal and 10% for the off-diagonal impedance components were used. The model mesh comprised 500 m cell widths between stations, resulting in x, y and z dimensions of 88, 84 and 44, respectively. The model took 97 days to complete 6 iterations, using 80 GB of memory. The final model yielded a normalized root mean squared (r.m.s.) misfit of 1.04. The overall fit to each impedance component for this model (Figure 3) indicates that each element is fit equally well and that residuals appear to follow a normal (Gaussian) distribution.

Normalized (by U_{max}) phase tensor difference ellipses for the WS-model are shown in Figure 4. This figure allows the data misfit to be systematically assessed in the frequency (period) - space domain, rather than relying on one value of overall misfit, which can be an unreliable diagnostic of a meaningful 3-D inversion model (Tietze and Ritter, 2013). Following Heise et al. (2013), with a suggested modification by Booker (2013), we have used the misfit tensor **U**,

$$\mathbf{U} = \mathbf{I} - \boldsymbol{\Phi}_{observed}\boldsymbol{\Phi}_{model}^{-1} \qquad (3.1)$$

to visualize the difference between the observed and modeled phase tensors. The misfit tensor ellipses in Figure 4 are filled with a colour that shows the Frobenious or Euclidean norm of **U**, which is the r.m.s. value of the components of **U**. This measure of the misfit equally weights all components and allows depiction of the misfit as a function of position and period. At short periods (T < 14s), the misfit ellipses are small and appear to be oriented randomly, indicating that the inversion model is fitting the dataset well. Misfits are larger at some sites at T = 3.5 s; expected since the data quality is lower in the period-band T ~ 1 – 10 s where the natural MT signal strength is weakest (e.g. Simpson and Bahr, 2005). At longer periods (T > 50 s), systematic patterns in the phase-tensor misfit ellipses appear, particularly at the edges of the data array. This effect may reflect the influence of structure outside the survey area where the inversion algorithm is less well constrained. Importantly, the misfit ellipse plots show no spatial correlation with high-voltage AC transmission-lines that transect the MT array, or indeed with the locations of high-temperature geothermal fields. In other words, key resistivity structures in the 3D WS-model that are associated with the locations of geothermal systems and discussed in previous publications (e.g. Bertrand et al., 2012; 2013) appear to be required by these data.

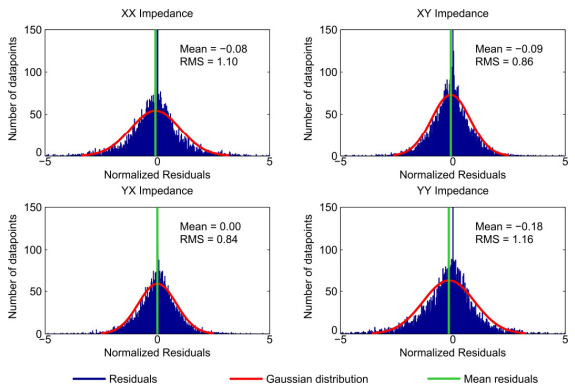

Figure 3: Misfit statistics of the tensor impedance components at all periods for the WS-model.

3.2 EMGeo-Model

The 3-D inversion algorithm EMGeo was also used to generate a resistivity model of a subset of the MT array data in the TVZ. Initial test models were generated to investigate the effects of the diagonal impedance components and model mesh coordinate frame. Subsequent models were generated using the full tensor impedance data in a geographic North-aligned coordinate system (i.e. rotated 45° with respect to the geoelectric strike of the TVZ and to the coordinate system used for the WS-model). To date, a coarse inversion model is complete, which inverted 8 periods (interpolated between the actual data) between 1 and 215 s, yielding an overall r.m.s. misfit of 2.5. The model mesh for this coarse inversion step used cell widths of 1 km (i.e. half the ~2 km station-spacing distance). Second-step inversion runs are planned that will add the shorter-period data on a refined mesh with 200-500 m cell widths between stations. The EMGeo inversion models were run using 1600-6000 CPU cores on the NERSC Cray XT4 Hopper system at LBNL, one of the largest scientific computing facilities in the world, shared by more than 5000 US-based researchers.

Several test models were generated using EMGeo to investigate the effects of different data-weighting and error-floor schemes. The results of these trials suggested down-weighting the impedance data with high variance and including an error floor of 15% for the diagonal and 3% for the off-diagonal components (N. Lindsey, personal communication, March 2014). Note for the EMGeo-model presented here, no assumptions were made regarding the geoelectric strike, and the error weighting scheme was applied in a geographic North-aligned coordinate system. In contrast, error floors in the WS-model were applied in a coordinate system aligned with the geoelectric strike of the TVZ (i.e. N45°E; e.g. Heise et al., 2007).

Phase-tensor misfit ellipses for the EMGeo-model are shown in Figure 5. As in the WS-model, higher misfit values are observed at 5 - 10 s periods where the MT signal-strength is weak. At mid-periods (e.g. T = 1 s), stations that show high misfits likely reflect the limited resolution of the coarse model mesh used. At 21 s period, relatively high misfit (10-15%) is observed for a band of stations aligned northeast-southwest, near the southeastern margin of the TVZ. Misfits are generally low for 46 s and 100 s periods, and increase at the longest period inverted (215 s) where the data quality is lower.

4. CONCLUSION

3-D inversion models generated using algorithms WSINV3DMT and EMGeo are shown for a 169-site subset of MT array data in the TVZ. By calculating phase tensor ellipses from each inversion model and computing phase tensor difference ellipses, we observe the overall misfit for each model. This approach permits a systematic assessment of the data misfit as a function of period and location that is independent of any galvanic distortion in the data.

Our analysis shows that the WS-model fits the measured data throughout the period-range inverted, and does not reveal patterns of high-misfit ellipses that strongly correlate with the locations of key model resistivity structures. The EMGeo-model shows a generally greater misfit than the WS-model. However, the EMGeo results represent a snapshot of work in progress and only used data from long periods on a coarse mesh. Future work will include the short period data on a refined model mesh.

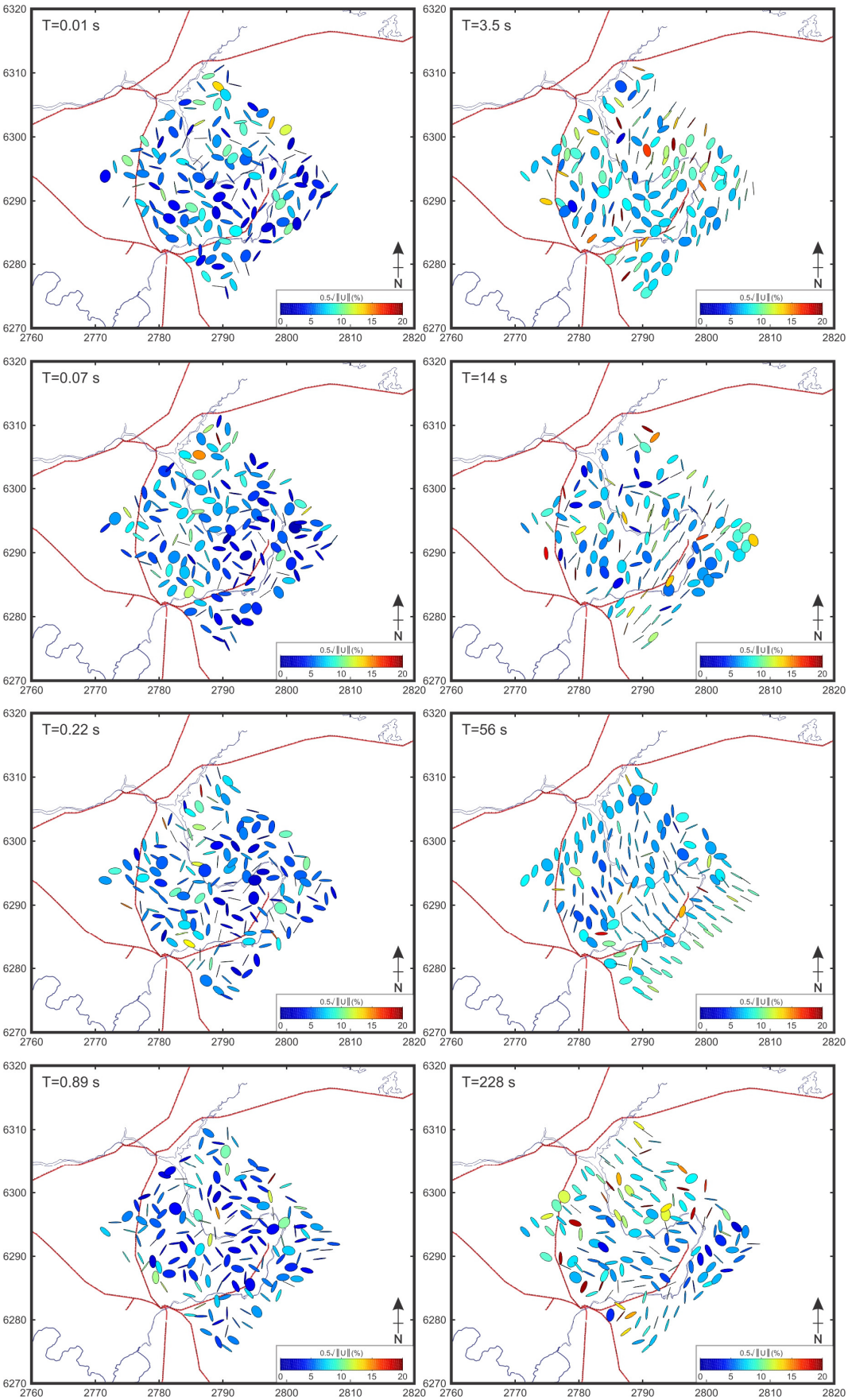

Figure 4: Phase tensor misfit ellipses for the WS-model showing the r.m.s. misfit of U, plotted as a percent and superimposed on a map of high-voltage power-lines (red) that intersect the MT array.

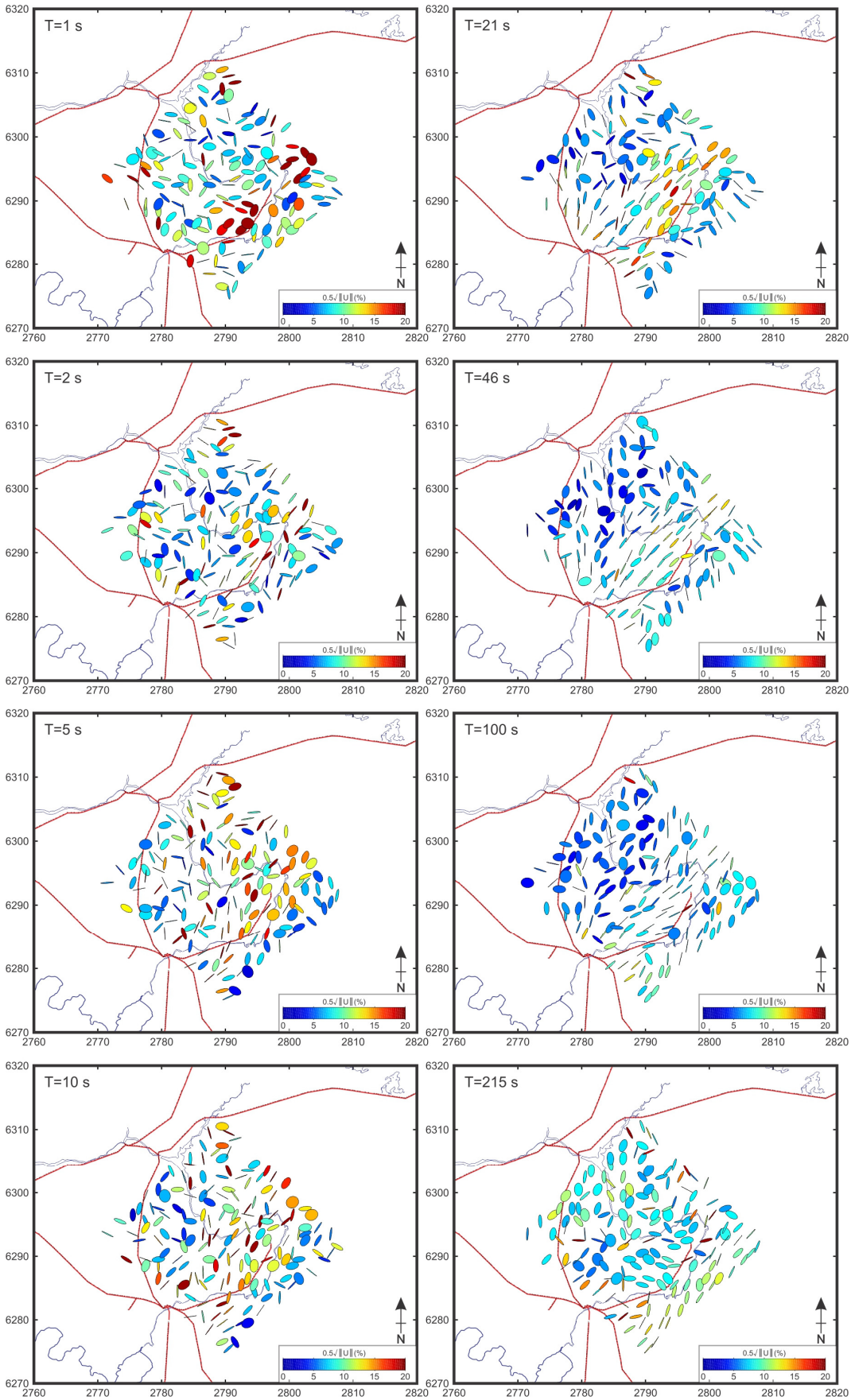

Figure 5: Phase tensor misfit ellipses for the EMGeo-model showing the r.m.s. misfit of U, plotted as a percent and superimposed on a map of high-voltage power-lines (red) that intersect the MT array.

ACKNOWLEDGEMENTS

Cooperation from landowners in the survey area is greatly appreciated. This project was supported by public research funding from the government of New Zealand. Additional funding was provided by the Bay of Plenty Regional Council and the Waikato Regional Council.

REFERENCES

Bertrand, E.A., Caldwell, T.G., Hill, G.J., Wallin, E.L., Bennie, S.L., Cozens, N., Onacha, S.A., Ryan, G.A., Walter, C., Zaino, A., and P. Wameyo, Magnetotelluric imaging of upper-crustal convection plumes beneath the Taupo Volcanic Zone, New Zealand: *Geophysical research letters, 39(2):* L02304, 2012.

Bertrand, E.A., Caldwell, T.G., Hill, G.J., Bennie, S.L. and S. Soengkono, Magnetotelluric imaging of the Ohaaki geothermal system, New Zealand: Implications for locating basement permeability: *Journal of Volcanology and Geophysical Research*, 268, 36-45, 2013.

Bahr, K., Interpretation of the Magnetotelluric impedance tensor: regional induction and local telluric distortion: *Journal of Geophysics*, 62, 119-127, 1988.

Bannister, S., Bourguignon, S., Sherburn, S. and E.A. Bertrand, Seismic imaging of the Central Taupo Volcanic Zone using double-difference tomography: *New Zealand Geothermal Workshop 2013 Proceedings*, 17-20 November 2013, Rotorua, New Zealand.

Bibby, H.M., T.G. Caldwell and C. Brown, Determinable and non-determinable parameters of galvanic distortion in Magnetotellurics: *Geophysical Journal International*, 163, 915-930, 2005.

Bibby, H.M., T.G. Caldwell, F.J. Davey and T.H. Webb, Geophysical evidence on the structure of the Taupo Volcanic Zone and its hydrothermal circulation: *Journal of Volcanology and Geothermal Research*, 68, 29-58, 1995.

Bignall, G., Hotter and deeper: New Zealand's research programme to harness its deep geothermal resources: *Proeedings World Geothermal Congress 2010*, Bali, Indonesia, 2010.

Booker, J.R., The magnetotelluric phase tensor: A critical review, *Surveys in Geophysics*, DOI 10.1007/s10712-013-9234-2, 2013.

Caldwell, T.G., H.M. Bibby and C. Brown, The magnetotelluric phase tensor: *Geophysical Journal International*, 158, 457-469, 2004.

Chave, A.D. and J.T. Smith, On electric and magnetic galvanic distortion tensor decomposition: *Journal of Geophysical Research*, 99, 4669-4682, 1994.

Groom, R.W. and R.C. Bailey, Decomposition of the Magnetotelluric impedance tensor in the presence of local three-dimensional galvanic distortion: *Journal of Geophysical Research*, 94, 1913-1925, 1989.

Heise, W., Bertrand, E.A., Caldwell, T.G., Hill, G.J., Palmer, N. and S. Bennie, Imaging the deep heat source of the Rotorua and Waimangu geothermal fields: *New Zealand Geothermal Workshop 2014 Proceedings*, 24-26 November, Auckland, New Zealand, 2014.

Heise, W., T.G. Caldwell, E.A. Bertrand, G.J. Hill, S.L. Bennie and Y. Ogawa, Changes in electrical resistivity track changes in tectonic plate coupling, *Geophysical Research Letters*, doi:10.1002/grl.50959, 2013.

Heise, W., T.G. Caldwell, H.M. Bibby and S.C. Bannister, Three-dimensional modeling of Magnetotelluric data from the Rotokawa geothermal field, Taupo volcanic zone, New Zealand: *Geophysical Journal International*, 173, 740-750, 2008.

Heise, W., H.M. Bibby, T.G. Caldwell, S.C. Bannister, Y. Ogawa, S. Takakura and T. Uchida, Melt distribution beneath a young continental rift: The Taupo volcanic zone, New Zealand: *Geophysical Research Letters*, 34, L14313, 2007.

Groom, R.W. and K. Bahr, Correction for near-surface effects: decomposition of the Magnetotelluric impedance tensor in the presence of local three-dimensional galvanic distortion: *Surveys in Geophysics*, 13, 341-379, 1992.

Jiracek, G.R., Near-surface and topographic distortions in electromagnetic induction: *Surveys in Geophysics*, 11, 163-203, 1990.

Ledo, J., 2-D versus 3-D magnetotelluric data interpretation: *Surveys in Geophysics*, 26, 671-806, 2005.

McNeice, G.W. and A.G. Jones, Multisite, multifrequency tensor decomposition of Magnetotelluric data, *Geophysics*, 66, 158-173, 2001.

Newman, G.A. and D.L. Alumbaugh, Three-dimensional magnetotelluric inversion using non-linear conjugate gradients: *Geophysical Journal* International, 140, 410-424, 2000.

Simpson, F. and K. Bahr, Practical Magnetotellurics: Cambridge University Press, Cambridge, 254 p, 2005.

Siripunvaraporn, W., G. Egbert, Y. Lenbury and M. Uyeshima, Three-dimensional Magnetotelluric inversion: data-space method: *Physics of the Earth and Planetary Interiors*, 150, 3-14, 2005.

Swift, C.M., A Magnetotelluric investigation of an electrical conductivity anomaly in the south western United States: *in* K. Vozoff ed., Magnetotelluric methods: Tulsa, Oklahoma, *Society of Exploration Geophysicists*, 156-166, 1986.

Swift, C.M., A Magnetotelluric investigation of an electrical conductivity anomaly in the south western United States: Ph.D. Thesis, *Massachusetts Institute of Technology*, Cambridge, Massachusetts, 230 p, 1967.

Tietze, K. and O. Ritter, Three-dimensional magnetotelluric inversion in practice – the electrical conductivity structure of the San Andreas fault in central California, *Geophysical Journal International*, doi:10.1093/gji/ggt234, 2013.

Tikhonov, A. N. and V.Y. Arsenin, Solutions of Ill-Posed Problems: V.H. Winston and Sons, Washington, D.C., 272 p, 1977.

Tuncer, V., M.J. Unsworth, W. Siripunvaraporn and J.A. Craven, Case History, Exploration for unconformity-type uranium deposits with audiomagnetotellurics data: A case study from the McArthur River mine, Saskatchewan, Canada: *Geophysics*, 71, B201-B209, 2006.

Unsworth, M.J., Magnetotelluric studies of active continent-continent collisions: *Surveys in Geophysics*, 31, 137-161, 2010.

Wannamaker, P.E., Affordable magnetotellurics: interpretation in natural environments: *in* M. Oristaglio and B. Spies, eds., Three-dimensional Electromagnetics: Geophysical Development Series, *Society of Exploration Geophysics*, Tulsa, Oklahoma, 7, 349-374, 1999.

Wannamaker, P.E., G.W. Hohmann and S.H. Ward, Magnetotelluric responses of three-dimensional bodies in layered earths: *Geophysics*, 49, 1517-1533, 1984.

Kelbert, A., Meqbel, N., Egbert, G.D. and K. Tandon, ModEM: A modular system for inversion of electromagnetic geophysical data: *Computers and Geosciences*, 66, 40-53, doi:10.1016/j.cageo.2014.01.010, 2014.

Egbert, G.D. and A. Kelbert, Computational Recipes for Electromagnetic Inverse Problems: *Geophysical Journal International*, 189, 251-267, doi:10.1111/j.1365-246X.2011.05347.x, 2012.

Wilson, C.J.N., B.F. Houghton, M.O. McWilliams, M.A. Lanphere, S.D. Weaver and R.M. Briggs, Volcanic and structural evolution of Taupo Volcanic Zone, New Zealand: a review: *Journal of Volcanology and Geothermal Research*, 68, 1-28, 1995.

Zhang, P., R.G. Roberts and L.B. Pedersen, Magnetotelluric strike rules: *Geophysics*, 52, 267-278, 1987.